Draft version April 5, 2016
Preprint typeset using LaTeX style emulateapj v. 03/07/07

DISCOVERY OF AN EXTRAORDINARY NUMBER OF RED SUPERGIANTS IN THE INNER GALAXY.

Maria Messineo[1,2], Qingfeng Zhu[1], Karl M. Menten[2], Valentin D. Ivanov[3], Donald F. Figer[4], Rolf-Peter Kudritzki[5], C.-H. Rosie Chen[2],
Draft version April 5, 2016

ABSTRACT

In this letter we present a search for Galactic red supergiant stars (RSGs) in the direction of the Inner Galaxy. A number of 94 targets selected from the 2MASS and GLIMPSE I North catalogs – via their blue extinction-free $Q1$ and $Q2$ colors – were spectroscopically observed at infrared wavelengths (in H and K band at R $\sim$ 1000) and an extraordinary high detection-rate of RSGs ($>$ 61%) was found. We identified spectroscopically 58 RSGs, **based on** their flat continua and large equivalent widths of the CO band at 2.293 μm (EW $>$ 45Å). This increase corresponds to about 25% of previously known RSGs in the Galactic region $10^\circ < l < 60^\circ$, $-1.^\circ1 < b < 1.^\circ1$. In order to confirm the location of the new RSGs in the Inner Galaxy, distances were estimated for a subsample of 47 stars with the clump method and found to range from 3.6 ± 0.4 to 8.6 ± 0.7 kpc. The large new sample will allow to investigate Galactic metallicity gradients as a function of galactocentric distances and azimuthal angles. Such information is currently an highly disputed issue to constrain models of Galaxy formation and evolution.

Subject headings: stars: evolution — infrared: stars — stars: supergiants — stars: massive — stars: abundances

1. INTRODUCTION

Massive stars are good tracers of Galactic plane morphology and kinematics; they serve to map the metallicity gradient and chemical enrichment of the Galaxy, and to provide constrains on the uncertain upper part of the stellar mass function (poorly populated because these stars are short lived). The detection of massive stars is hampered by our unlucky position in the Disk, and, consequently, the high degree of (patchy) interstellar extinction (e.g., Messineo et al. 2010, 2011).

In the last decade, several massive clusters rich in red supergiants (RSGs) were discovered between $l = 26^\circ$ and 30°, at a distance of $\approx$ 6 kpc; they contain 14, 26, $>$ 16, $>$ 13, and 7 RSGs, respectively (e.g., Figer et al. 2006; Davies et al. 2007; Clark et al. 2009; Negueruela et al. 2010, 2011), and are called RSGC clusters (RSGC1, RSGC2, RSGC3, RSGC4, and RSGC5). Their combined star forming activity constitutes a starburst that has a mass comparable to that of the Galactic center region, and they form the highest concentration of RSGs known in the Galaxy (they represent ≈30% of RSGs known at $10^\circ < l < 60^\circ$, $-1.^\circ1 < b < 1.^\circ1$). It is most **likely located at a** Galactocentric radius of 3.5 kpc, at a location at which the near-end side of the Galactic Bar appears to interact with the Scutum-Centaurus spiral arm (e.g., Davies et al. 2009b; Habing et al. 2006).

This starburst could be a density peak of a large population of Disk RSGs, maybe in a ring-like structure surrounding the central Bar or in a more prominent arm. Rings of increased massive star formation are often observed in external galaxies, as well as concentrations of massive clusters at the intersection points of such rings and arms with bars (e.g., Davies et al. 2009b; Mazzuca et al. 2008). The Milky Way is a barred spiral galaxy, most likely with 4 arms (e.g., Benjamin et al. 2005; Drimmel & Spergel 2001); a possible ring structure at corotation has often been invoked, for example to explain stellar counts of giant stars and the luminosity function of HII regions (e.g., Comeron & Torra 1996; Bertelli et al. 1995a,b).

Our current knowledge on the Galactic distribution of RSGs is hampered by incompleteness, poor statistics, and lack of distances. Only $\sim$ 1000 Galactic RSGs out of a predicted population of at least 5000 RSGs are currently known (e.g., Gehrz 1989). To put the likely association of such a concentration of RSGCs with the near-endside of the Bar in perspective, further searches for RSGs at positive Galactic longitudes are needed. A 3D mapping of RSGs in the inner Galaxy is possible for individually detected RSGs at moderate interstellar extinction (e.g., the near side), by using clump stars as distance indicators (Messineo et al. 2014b). We, therefore, carried out a search for RSGs from the GLIMPSE I North catalog (Churchwell et al. 2009; Benjamin et al. 2003) and the 2MASS catalog (Skrutskie et al. 2006).

In Sect. 2, we describe the sample, and in Sect. 3 the spectroscopic observations and data reduction. The spectra are analyzed in Sect. 4, and distances estimated in Sect. 4.2.1. The results are summarized in Sect. 5.

2. THE SAMPLE SELECTION

We selected candidate RSGs by using a set of color criteria based on 2MASS and GLIMPSE data (Messineo et al. 2005, 2012, and references therein). They are based on the $Q1$ and $Q2$ parameters **and are independent of** interstellar extinction. $Q1$ is a function of J, H and K_s magnitudes, while $Q2$ is defined as a function of J, K_s, and [8μm] magnitudes. The region $0.1 < Q1 < 0.5$ mag and $0.5 < Q2 < 1.5$ mag encloses 42% of the known RSGs (Messineo et al. 2014a,b).

By using this **criterion** and an initial $K_s <$ 7 mag, we pre-selected 8813 point sources from the Version 2.0 of the **GLIMPSE I North** data release. By imposing $A_{K_s} > 0.4$ mag and a minimum luminosity ($M_{bol} < -6.1$ mag) for an initial assumed distance of 4 kpc (i.e., $K_s < 4 + A_{K_s}$), and good photometric quality, we reduced the sample down to 128 obscured-far-luminous stars, of which we observed 94 stars. The targets

[1] Key Laboratory for Researches in Galaxies and Cosmology, University of Science and Technology of China, Chinese Academy of Sciences, Hefei, Anhui, 230026, China
[2] Max-Planck-Institut für Radioastronomie, Auf dem Hügel 69, D-53121 Bonn, Germany
[3] European Southern Observatory, Karl Schwarzschild-Strasse 2, D-85748 Garching bei Munchen, Germany
[4] Center for Detectors, Rochester Institute of Technology, 54 Memorial Drive, Rochester, NY 14623, USA
[5] Institute for Astronomy, University of Hawaii, 2680 Woodlawn Drive, Honolulu, HI 96822

are located between l = 10° and 70° (GLIMPSE I North, Benjamin et al. 2003; Churchwell et al. 2009).

3. OBSERVATION AND DATA REDUCTION

Spectroscopic observations were carried out with the SofI (Son of ISAAC, Moorwood et al. 1998) Spectrograph on the ESO/NTT (New Technology Telescope) 3.58m telescope of the La Silla Observatory, **on the three nights from UT June 16th to 19th, 2015** – program ID 095.D-0252(A).

Spectra with the low-resolution **red** grism, and the 0.″6 wide slit, delivering resolution R ~ 980 over the wavelength range λ=1.53–2.52 μm were obtained for 94 targets. For each target a minimum number of four exposures, nodded along the slit, were taken in an ABBA sequence. Typical integration times per frame ranged from 2 to 100 s (DITs×NDITs).

Data reduction was performed with IDL scripts and with the Image Reduction and Analysis Facility software (IRAF[6]). Pairs of consecutive exposures were subtracted one from another and flat-fielded (with spectroscopic lamp flats). Traces were located in each reduced exposure. Xenon arc spectra (for the dispersion axis) and traces (for the spatial axis) were used to linearize the traces. For each target, traces were extracted from the reduced exposures, wavelength calibrated with lamp arcs, linearly dispersed in wavelength, and **averaged** combined with a 3 σ clipping.

Corrections for atmospheric transmission and instrumental response were done by dividing the spectra by a telluric standard (typically a B-type star) – taken at similar airmass as and within 1 hour from the target observation – and by multiplying them by a black body curve (at the temperature of the standard). **A list of the 94 observed targets is provided in the electronic Table 1.**

4. ANALYSIS

4.1. *CO equivalent widths and water indexes*

In the works of Figer et al. (2006) and Messineo et al. (2014b) we demonstrated that low-resolution (R=1000) *HK* spectra allow to spectrally classify late-type stars within two subclasses and to separate RSGs from asymptotic giant branch stars (AGBs).

Spectra were corrected for interstellar extinction (Messineo et al. 2005) with an average $(J-K_s)_o$= 1.05 mag and $(H-K_s)_o$ = 0.23 mag (this yields an initial A_{K_s} uncertainty of 0.075 mag, negligible for spectral classification). For the equivalent width of the CO-band at 2.293 μm, the continuum was selected in the range 2.28-2.29 μm, while the CO-band was measured in the range 2.285-2.315 μm. The median of the errors, estimated by shifting the continuum region, is 0.8 Å. Since giants and supergiants follow two different EW(CO)-versus-temperature relations, and giants have a narrower range of EW(CO)s than RSGs (see Fig. 1), we were able to identify late-type RSGs ($\gtrsim$ M0 I).

Mira AGB stars have generally strong water absorption at the two edges of the *H* and *K*-bands due to H_2O in their envelopes, and especially their *H*-band spectra may display a highly curved continuum (e.g. Lançon & Wood 2000). In order to distinguish between RSGs and Mira AGBs, we analyzed the shape of the dereddened spectra, and measured the depth of the H_2O **absorption. The water index is defined as in Blum et al. (2003), with the water band at 2.0525-2.0825 μm and two continuum bands at 1.68-1.72 μm and**

[6] **IRAF is distributed by the National Optical Astronomy Observatories, which is operated by the Association of Universities.**

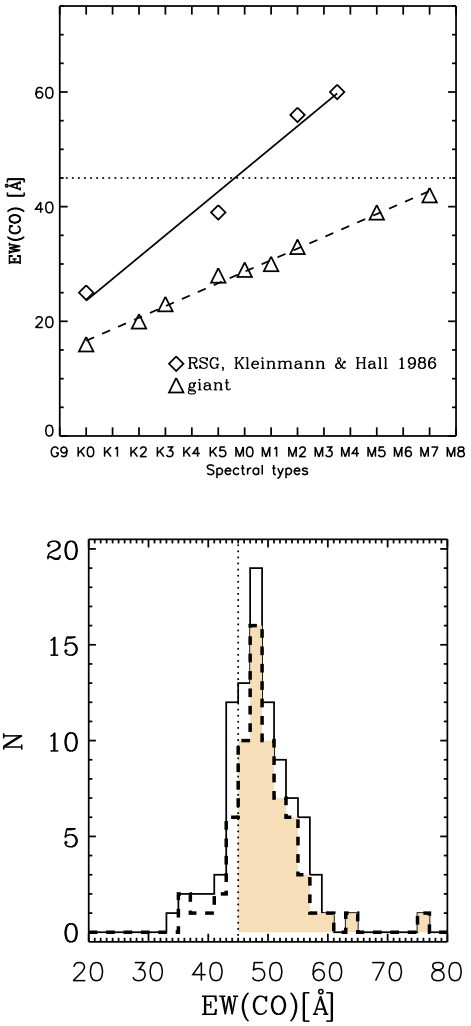

FIG. 1.— *Top:* Measurements of EW(CO)s for template spectra taken from Kleinmann & Hall (1986). Giants have EWs below 45Å (horizontal line). *Bottom:* Histogram of EW(CO)s from the sample of 94 GLIMPSE targets (solid line). The long-dashed line shows a reduced sample, without the 12 stars with uncertain water measures and 14 stars with moderate water content. The vertical dashed line (EW=45Å) marks the adopted limit to classify highly-probable RSGs. Histograms are **built** with a bin of 2Å.

2.20-2.29 μm. Index= $(100 * (1 - < F_{H_2O}/F_{cont} >))$**, where F_{H_2O} is the observed flux density and F_{cont} is a fitted flux density with a bilinear fit to the two continua.**

Water indexes range from −4.3% to 14.8% (see Fig. 2). For each star, a typical random scatter within 4.8% was measured with individual exposures. A total of 12 stars were not classified since their random scatters exceeded the estimated 1 σ for a gaussian distribution.

4.2. *Spectroscopic RSGs*

The resulting water indexes and EW(CO)s of targeted stars are shown in Fig. 2, along with comparison values derived with the IRTF spectral library (Rayner et al. 2009; Messineo et al. 2014b). Known classical Mira AGBs have an H_2O index larger than 15%, semiregular (SR) AGBs and RSGs smaller than 10% (e.g. Blum et al. 2003; Messineo et al. 2014b). Since SR variables appear to have EW(CO) < 44 Å, we conservatively call highly-probable RSGs those targets with H_2O indexes smaller than 7.5% and EW(CO) > 45Å.

The sample contains an extraordinarily large number of

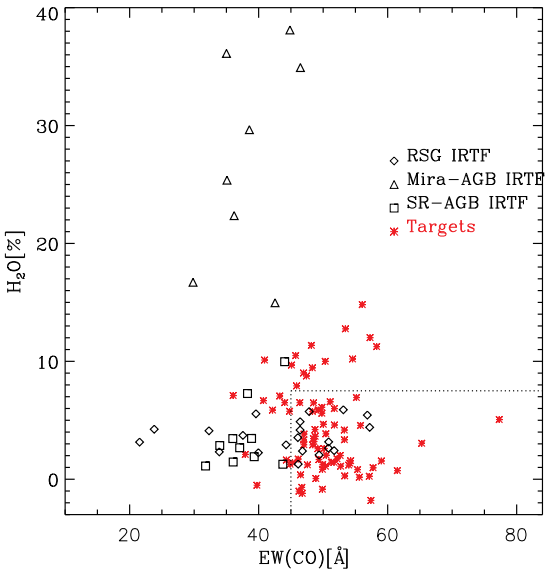

FIG. 2.— H_2O indexes versus EW(CO)s of the observed targets (asterisks). For comparison, similar measurements **were extracted from** spectra of AGBs (Miras and semiregulars **marked** with triangles and squares) and RSGs (diamonds) of the IRTF library (Rayner et al. 2009), **and here** shown. The dotted box encloses the targets classified as spectroscopic RSGs.

highly-probable RSGs, 58 out of 94 stars. Among the remaining, a number of 14 stars show moderate water absorption (7.5% <H_2O< 15%), but there are no Miras (H_2O > 15%).

4.2.1. *Distances*

For a subsample of 68 observed targets, including 47 spectroscopic RSGs, **distances can be inferred using nearby red clump stars as primary indicators** (e.g. Messineo et al. 2014b). **We used the method of Drimmel et al. (2003). We selected by eyes well visible clump sequences, and analyzed their K magnitudes per bin of $J-K$ color. The peak magnitude was measured with a Gaussian fit. We used an intrinsic $(J-K)_o$ of 0.68 mag (Babusiaux & Gilmore 2005; Gonzalez et al. 2011) and an absolute magnitude in K-band of −1.61 mag (Alves 2000). Reported values range from M_K=−1.54, −1.55 mag to M_K=−1.72 mag (Messineo et al. 2014b, and references therein).** Typically, with UKIDSS $(J-K, K)$ color-magnitude diagrams (Lucas et al. 2008) and fields of $10' \times 10'$, centred on the targets, the location of the mean clump sequence can be traced quite accurately (0.15 mag). The clump sequence allows us to derive distances as a function of interstellar extinction along each line of sight. The target distance modulus (DM) is estimated by matching the value of interstellar extinction of each target with that of clump stars along the line of sight. In Fig. 3 we show a few examples of clump sequences with 2MASS-UKIDSS data[7]. **Since we targeted stars with K_s< 4+A_{K_s}, as a result, absolute K_s magnitudes decrease with increasing $(J-K_s)$.**

5. DISCUSSION AND CONCLUSIONS

A number of 94 stars with 2MASS-GLIMPSE colors typical of Galactic RSGs were spectroscopically observed at infrared wavelengths. Spectroscopic infrared measurements of water absorption and EWs of CO molecular bands have confirmed that 58 of these are highly-probably RSGs.

[7] **No corrections were applied between the UKIDSS photometric system (J,K) and 2MASS system (J,K_s) (Hodgkin et al. 2009); K UKIDSS and K_s 2MASS are within 0.01 mag and J UKIDSS − J 2MASS within 0.05 mag.**

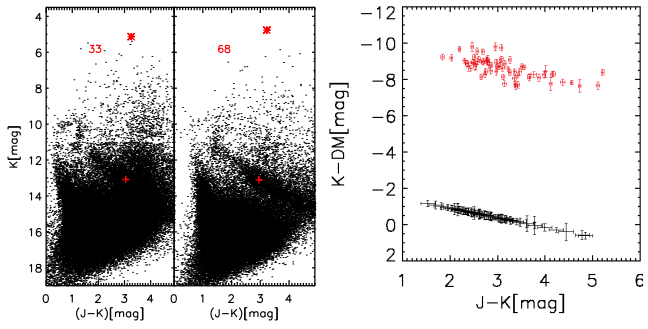

FIG. 3.— *Left:* $J-K$ versus K diagrams of UKIDSS data (Lucas et al. 2008) in $10' \times 10'$ fields centred on the #33 and #68 targets (asterisks). Identification numbers are taken from Table 1. 2MASS J,K_s data are used above K_s= ∼ 11 mag. Crosses mark **the location of the peak of clump star counts** with an A_K within ±0.15 mag of that of the target. *Right:* 2MASS K_s-DM of targets versus their J-K_s colors. Average UKIDSS K-DM and $(J-K)$ values of field clump stars with A_K within ±0.15 mag that of the target are shown at the bottom.

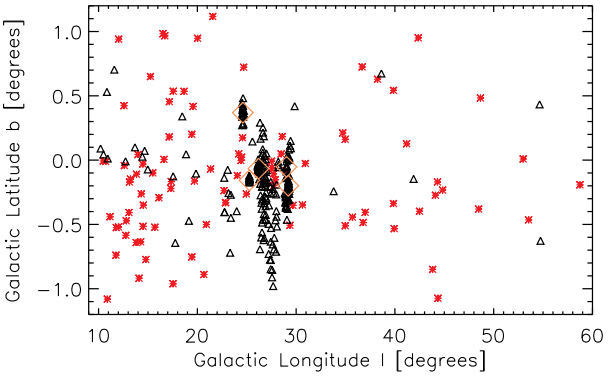

FIG. 4.— Distribution of RSGs in Galactic coordinates, (l, b), of the observed targets (asteriks). For comparison, we mark with diamonds the location of the five massive **RSGCs** located between l=25° and l=30°, at the near-end of the Galactic Bar. Previously, known RSG stars are marked with open triangles (Skiff 2014; Comerón et al. 2004; Negueruela et al. 2010, 2011; Clark et al. 2009; Verheyen et al. 2012; Messineo et al. 2008).

The longitude-latitude distribution of the new sample of RSGs is shown in Fig. 4, along with other sources classified as RSGs (mostly from Skiff 2014). We have increased the number of known RSGs in the range $10° < l < 60°$, $-1.^\circ1 < b < 1.^\circ1$ at least by 25% – by only considering the sample of spectroscopic RSGs. For a subsample of 47 new RSGs, distances were inferred with red clump stars at similar interstellar extinction as the target (Messineo et al. 2014b). The distribution of the observed targets on the XY plane is shown in Fig. 5; they appear located in the inner Galaxy at Galactocentric distances between ∼ 3 and ∼ 7 kpc, while the **RSGCs** are at a distances of 4-4.5 kpc.

Our current knowledge on the distribution of RSGs in the Milky Way and on Galactic metallicity gradients traced with RSGs is **scarce**. Studies of abundances in RSGs of the RSGCs have reported anomalous subsolar metallicities in disagreement with those from Cepheids (Davies et al. 2009b; Origlia et al. 2016). However, because of poor statistics the authors were not able to distinguish between stochastic fluctuation of metallicity from cloud to cloud, systematic bias in the measurements, and/or real trends with Galactocentric distances and azimuthal positions. The newly discovered GLIMPSE RSGs towards the inner Galaxy uniquely have the potential

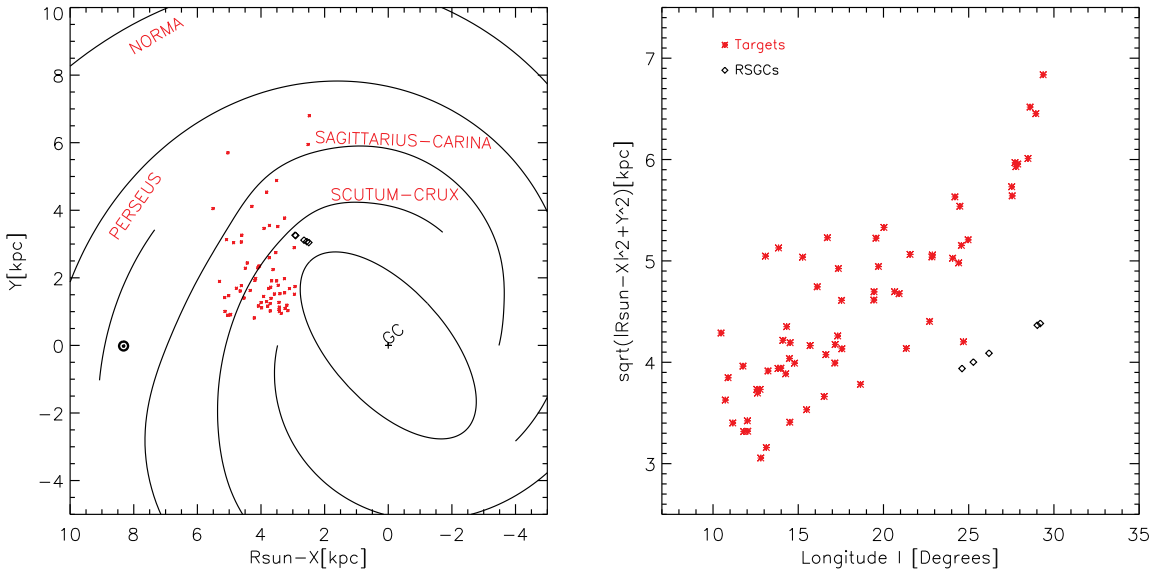

FIG. 5.— *Left:* XY distribution of observed targets (asterisks) on the plane of the Milky Way. As a comparison the five RSGCs between 25° and 30° of longitudes are marked with diamonds. The Sun is at (0.0,8.5) and the Galactic center is at (0,0). Spiral arms are taken from the work of Cordes & Lazio (2002). The central bar is sketched as an ellipse with a major axis of 3.5 kpc. *Right:* Galactocentric distances versus longitudes.

to address this metallicity issue. They represent an homogeneously selected sample of RSGs; they go 1 kpc closer to the GC than the RSGCs and are distributed over a larger range of longitudes. In conclusion, they may serve as a bridge between the RSGs in the RSGCs at the near endside of the Galactic Bar (l=25-30°) and those in the 200 pc central ring of the Milky Way (l=±1.5°) (Davies et al. 2009b,a; Habing et al. 2006). We plan to extend this search for RSGs to the central 10° of longitudes with the **GLIMPSE II and GLIMPSE3D** catalogs (Churchwell et al. 2009).

Some new RSGs are associated with the Sagittarius-Carina and Scutum-Crux arms, as shown in Figure 5. There is a concentration of 24 of them between 3 < X < 4 kpc and 1 < Y < 2 Kpc (l from 10° to 22°); this concentration appears at the top of the innermost (Norma) spiral arm or may be part of a ring that meets the tip of the bar at 25–30 ° (see for example Sanna et al. 2014).

Most of the new RSGs will not be detectable with **Gaia** because of their faint V-magnitudes in crowded regions. Since kinematic velocities cannot be regarded as primary indicators of distances for objects in the central 4 kpc where non-circular motions are dominant (due to the presence of the Bar), photometric monitoring could provide independent measures of distances for those far-obscured RSGs that periodically pulsate and are not members of clusters.

MM thanks H. Habing, E. Churchwell, B. Davies, and T. Kaminski for inspiring discussions on GLIMPSE data, Galactic stars. We are thankful to the SofI team for a great support. This publication makes use of data products from the Two Micron All Sky Survey, which is a joint project of the University of Massachusetts and the Infrared Processing and Analysis Center/California Institute of Technology, funded by the National Aeronautics and Space Administration and the National Science Foundation. This work is based on observations made with the Spitzer Space Telescope, which is operated by the Jet Propulsion Laboratory, California Institute of Technology under a contract with NASA. This work is based on data obtained as part of the UKIRT Infrared Deep Sky Survey. This research has made use of the VizieR catalogue access tool, CDS, Strasbourg, France, and SIMBAD database. This research has made use of NASAs Astrophysics Data System Bibliographic Services. This work was partially supported by the ERC Grant GLOSTAR (247078), by the Fundamental Research Funds for the Central Universities in China, and USTC grant KY2030000054.

REFERENCES

Alves, D. R. 2000, ApJ, 539, 732
Babusiaux, C. & Gilmore, G. 2005, MNRAS, 358, 1309
Benjamin, R. A., Churchwell, E., Babler, B. L., et al. 2003, PASP, 115, 953
Benjamin, R. A., Churchwell, E., Babler, B. L., et al. 2005, ApJ, 630, L149
Bertelli, G., Bressan, A., Chiosi, C., Ng, Y. K., & Ortolani, S. 1995a, A&A, 301, 381
Bertelli, G., Bressan, A., Chiosi, C., Ng, Y. K., & Ortolani, S. 1995b, A&A, 301, 381
Blum, R. D., Ramírez, S. V., Sellgren, K., & Olsen, K. 2003, ApJ, 597, 323
Churchwell, E., Babler, B. L., Meade, M. R., et al. 2009, PASP, 121, 213
Clark, J. S., Negueruela, I., Davies, B., et al. 2009, A&A, 498, 109
Comeron, F. & Torra, J. 1996, A&A, 314, 776
Comerón, F., Torra, J., Chiappini, C., et al. 2004, A&A, 425, 489
Cordes, J. M. & Lazio, T. J. W. 2002, Astrophysics e-prints: astro-ph/0207156
Davies, B., Figer, D. F., Kudritzki, R.-P., et al. 2007, ApJ, 671, 781
Davies, B., Origlia, L., Kudritzki, R.-P., et al. 2009a, ApJ, 694, 46
Davies, B., Origlia, L., Kudritzki, R.-P., et al. 2009b, ApJ, 696, 2014
Drimmel, R., Cabrera-Lavers, A., & López-Corredoira, M. 2003, A&A, 409, 205
Drimmel, R. & Spergel, D. N. 2001, ApJ, 556, 181
Figer, D. F., MacKenty, J. W., Robberto, M., et al. 2006, ApJ, 643, 1166
Gehrz, R. 1989, in IAU Symposium, Vol. 135, Interstellar Dust, ed. L. J. Allamandola & A. G. G. M. Tielens, 445
Gonzalez, O. A., Rejkuba, M., Zoccali, M., Valenti, E., & Minniti, D. 2011, A&A, 534, A3
Habing, H. J., Sevenster, M. N., Messineo, M., van de Ven, G., & Kuijken, K. 2006, A&A, 458, 151
Hodgkin, S. T., Irwin, M. J., Hewett, P. C., & Warren, S. J. 2009, MNRAS, 394, 675
Kleinmann, S. G. & Hall, D. N. B. 1986, ApJS, 62, 501
Lançon, A. & Wood, P. R. 2000, A&AS, 146, 217
Lucas, P. W., Hoare, M. G., Longmore, A., et al. 2008, MNRAS, 391, 136
Mazzuca, L. M., Knapen, J. H., Veilleux, S., & Regan, M. W. 2008, ApJS, 174, 337
Messineo, M., Davies, B., Figer, D. F., et al. 2011, ApJ, 733, 41

TABLE 1
LIST OF OBSERVED SELECTED STARS.

ID	RA(J2000) [hh mm ss]	DEC(J2000) [° ′ ″]	H_2O %	EW(CO) [Å]	Sp[rsg]	Sp[giant]
1	18 08 28.19	−18 03 07.48	8.8 ± 3.0	47.4 ± 1.4	M0.5	M7
2	18 08 45.56	−19 52 54.99	14.8 ± 0.3	56.1 ± 0.8	M2.5	..
3	18 09 17.11	−19 39 58.81	10.2 ± 1.1	54.6 ± 1.5	M2	..
4	18 11 27.29	−17 50 14.10	6.5 ± 4.2	48.5 ± 0.5	M0.5	M7
5	18 11 47.36	−19 29 15.68	3.3 ± 0.6	53.3 ± 2.3	M2	..
6	18 13 15.62	−18 01 22.48	6.6 ± 3.0	51.1 ± 0.3	M1	..
7	18 13 23.42	−18 58 18.66	2.1 ± 0.8	37.9 ± 2.2	K4	M4.5
8	18 13 36.72	−20 02 13.15	11.0 ± 6.6	38.7 ± 0.6	K4	M5
9	18 13 49.15	−18 46 33.37	2.9 ± 3.7	47.0 ± 0.7	M0	M7
10	18 14 06.83	−19 06 20.44	5.7 ± 2.8	48.3 ± 0.5	M0.5	M7
11	18 14 45.94	−17 37 54.96	2.6 ± 0.4	50.2 ± 0.6	M1	..
12	18 14 52.70	−17 32 00.19	9.4 ± 1.5	48.3 ± 0.4	M0.5	M7
13	18 15 13.56	−18 03 40.54	10.0 ± 1.1	50.3 ± 0.7	M1	..
14	18 15 32.37	−17 47 22.01	12.0 ± 1.4	57.3 ± 1.9	M3	..
15	18 15 33.76	−18 09 04.81	11.4 ± 3.3	48.2 ± 1.1	M0.5	M7
16	18 15 41.13	−16 46 45.73	2.0 ± 4.6	52.6 ± 1.3	M1.5	..
17	18 15 58.32	−16 58 27.87	2.6 ± 2.0	49.2 ± 1.5	M0.5	M7
18	18 15 59.61	−15 22 08.72	2.2 ± 5.3	44.9 ± 0.5	K5.5	M7
19	18 16 57.20	−16 22 23.59	4.1 ± 8.4	56.6 ± 0.9	M2.5	..
20	18 17 15.99	−14 05 54.35	1.2 ± 4.4	47.6 ± 0.4	M0.5	M7
21	18 17 28.65	−16 37 39.96	1.3 ± 3.5	44.9 ± 0.6	K5.5	M7
22	18 17 41.60	−13 56 28.05	0.4 ± 2.5	46.5 ± 1.5	M0	M7
23	18 17 52.12	−17 15 08.51	1.6 ± 0.5	54.3 ± 0.7	M2	..
24	18 18 12.56	−16 29 13.26	−4.3 ± 7.9	52.8 ± 1.8	M1.5	..
25	18 18 44.53	−16 51 08.98	−1.2 ± 1.9	46.8 ± 0.9	M0	M7
26	18 18 46.60	−16 34 56.69	0.2 ± 2.5	57.2 ± 0.7	M3	..
27	18 19 11.37	−15 31 09.96	12.0 ± 10.4	58.9 ± 4.8	M3.5	..
28	18 19 27.24	−17 07 59.29	8.3 ± 6.4	35.3 ± 1.4	K3	M3.5
29	18 20 16.13	−16 27 41.53	7.1 ± 2.7	43.3 ± 0.4	K5	M7
30	18 20 26.51	−13 46 48.69	4.6 ± 7.1	42.6 ± 0.8	K5	M7
31	18 20 54.67	−13 23 41.59	9.4 ± 7.1	47.8 ± 1.1	M0.5	M7
32	18 21 00.94	−14 28 20.90	2.9 ± 12.1	51.6 ± 1.2	M1.5	..
33	18 21 06.86	−15 03 40.20	3.2 ± 0.6	48.6 ± 1.0	M0.5	M7
34	18 21 08.46	−15 32 09.10	3.0 ± 0.9	65.3 ± 0.8	M5	..
35	18 21 24.28	−13 55 28.16	3.6 ± 1.4	48.8 ± 0.3	M0.5	M7
36	18 23 01.08	−12 25 53.83	6.4 ± 8.7	44.5 ± 1.0	K5.5	M7
37	18 23 04.12	−13 54 16.05	1.4 ± 1.8	54.2 ± 0.5	M2	..
38	18 23 11.20	−13 57 58.05	1.7 ± 1.5	49.3 ± 0.3	M1	M7
39	18 24 09.91	−11 01 21.55	−4.2 ± 4.1	45.1 ± 0.9	K5.5	M7
40	18 25 11.21	−11 40 56.73	4.2 ± 4.8	53.3 ± 0.6	M2	..
41	18 25 43.82	−11 53 36.90	1.7 ± 3.0	46.1 ± 2.4	M0	M7
42	18 26 19.22	−14 06 48.76	−1.8 ± 3.7	57.4 ± 0.6	M3	..
43	18 26 27.72	−9 35 18.97	−0.5 ± 0.9	39.7 ± 0.6	K4	M5.5
44	18 27 33.54	−11 49 27.02	−1.0 ± 7.0	45.9 ± 0.5	M0	M7
45	18 29 12.34	−12 19 40.85	−0.7 ± 2.3	46.7 ± 0.9	M0	M7
46	18 30 18.90	−10 20 00.36	3.8 ± 4.4	47.0 ± 1.2	M0	M7

Messineo, M., Figer, D. F., Davies, B., et al. 2010, ApJ, 708, 1241
Messineo, M., Figer, D. F., Davies, B., et al. 2008, ApJ, 683, L155
Messineo, M., Habing, H. J., Menten, K. M., et al. 2005, A&A, 435, 575
Messineo, M., Menten, K. M., Churchwell, E., & Habing, H. 2012, A&A, 537, A10
Messineo, M., Menten, K. M., Figer, D. F., et al. 2014a, A&A, 569, A20
Messineo, M., Zhu, Q., Ivanov, V. D., et al. 2014b, A&A, 571, A43
Moorwood, A., Cuby, J.-G., & Lidman, C. 1998, The Messenger, 91, 9
Negueruela, I., González-Fernández, C., Marco, A., & Clark, J. S. 2011, A&A, 528, A59
Negueruela, I., González-Fernández, C., Marco, A., Clark, J. S., & Martínez-Núñez, S. 2010, A&A, 513, A74
Origlia, L., Oliva, E., Sanna, N., et al. 2016, A&A, 585, A14
Rayner, J. T., Cushing, M. C., & Vacca, W. D. 2009, ApJS, 185, 289
Sanna, A., Reid, M. J., Menten, K. M., et al. 2014, ApJ, 781, 108
Skiff, B. A. 2014, VizieR Online Data Catalog, 1, 2023
Skrutskie, M. F., Cutri, R. M., Stiening, R., et al. 2006, AJ, 131, 1163
Verheyen, L., Messineo, M., & Menten, K. M. 2012, A&A, 541, A36

TABLE 1
CONTINUATION OF TABLE 1.

ID	RA(J2000) [hh mm ss]	DEC(J2000) [° ′ ″]	H_2O %	EW(CO) [Å]	Sp[rsg]	Sp[giant]
47	18 31 04.61	−10 54 26.04	5.6 ± 1.4	49.8 ± 0.6	M1	M7
48	18 31 58.82	−11 19 21.37	6.5 ± 1.5	46.4 ± 0.8	M0	M7
49	18 33 28.70	−9 12 09.19	11.2 ± 1.1	58.3 ± 0.4	M3	..
50	18 33 44.45	−6 59 47.41	6.1 ± 2.9	49.8 ± 0.7	M1	M7
51	18 34 04.71	−9 07 17.67	9.0 ± 1.7	47.0 ± 2.2	M0	M7
52	18 34 07.13	−9 05 53.58	12.8 ± 0.8	53.5 ± 1.0	M2	..
53	18 35 13.47	−7 44 58.14	6.7 ± 4.1	40.7 ± 1.1	K4.5	M6
54	18 35 29.03	−7 21 12.60	6.9 ± 4.6	55.2 ± 0.8	M2.5	..
55	18 35 34.76	−7 56 48.52	3.3 ± 1.8	47.0 ± 1.5	M0	M7
56	18 35 49.12	−7 34 43.09	0.8 ± 1.8	49.9 ± 0.5	M1	M7
57	18 35 51.52	−7 30 11.36	1.5 ± 0.4	59.0 ± 0.6	M3.5	..
58	18 37 46.52	−7 12 24.60	6.0 ± 2.4	51.7 ± 0.5	M1.5	..
59	18 41 34.82	−4 48 58.00	1.4 ± 3.1	51.3 ± 0.4	M1.5	..
60	18 41 48.35	−4 48 52.91	1.7 ± 3.1	52.2 ± 0.6	M1.5	..
61	18 42 17.11	−4 41 16.98	1.1 ± 1.0	52.7 ± 0.8	M1.5	..
62	18 42 42.31	−4 40 53.36	1.0 ± 1.0	57.7 ± 0.4	M3	..
63	18 42 44.80	−4 33 57.39	4.2 ± 4.3	48.7 ± 1.1	M0.5	M7
64	18 42 52.23	−3 46 18.48	0.2 ± 1.1	55.6 ± 0.7	M2.5	..
65	18 43 08.01	−3 56 24.05	0.8 ± 0.4	55.3 ± 0.9	M2.5	..
66[a]	18 44 26.16	−3 35 27.61	0.1 ± 3.8	48.9 ± 0.7	M0.5	M7
67	18 46 44.42	−3 24 04.96	0.7 ± 1.3	61.5 ± 0.6	M4	..
68	18 46 44.80	−3 03 32.19	1.2 ± 3.1	54.0 ± 0.4	M2	..
69	18 47 53.58	−1 47 15.08	0.3 ± 2.3	53.3 ± 0.5	M2	..
70	18 48 29.97	−2 11 50.01	1.4 ± 1.4	51.7 ± 0.6	M1.5	..
71	18 53 57.32	1 41 27.11	5.9 ± 2.8	42.2 ± 0.6	K5	M6.5
72	18 54 34.44	1 53 04.60	4.7 ± 1.6	50.0 ± 0.8	M1	..
73	18 55 42.14	3 40 04.56	10.5 ± 1.6	45.7 ± 0.4	M0	M7
74	18 56 58.50	1 34 52.05	1.1 ± 2.2	50.4 ± 0.5	M1	..
75	18 58 04.34	2 15 41.31	3.5 ± 4.8	48.5 ± 0.5	M0.5	M7
76	18 58 53.84	5 00 36.87	7.1 ± 2.3	36.0 ± 1.7	K3.5	M3.5
77	19 00 12.29	3 12 25.93	1.2 ± 1.4	49.9 ± 0.8	M1	M7
78	19 00 18.13	3 25 41.33	5.9 ± 2.8	49.2 ± 0.5	M0.5	M7
79	19 02 10.62	6 24 27.06	5.8 ± 2.5	44.8 ± 0.9	K5.5	M7
80	19 05 19.33	6 00 12.65	6.5 ± 1.6	44.0 ± 0.3	K5.5	M7
81	19 05 20.11	8 48 57.14	7.9 ± 2.7	45.9 ± 0.4	M0	M7
82	19 06 07.20	7 23 54.59	10.1 ± 1.7	40.9 ± 1.4	K4.5	M6
83	19 06 09.34	5 58 44.39	1.4 ± 1.6	45.2 ± 1.4	K5.5	M7
84	19 10 25.67	8 18 52.38	3.8 ± 2.9	50.4 ± 0.6	M1	..
85	19 12 59.96	9 48 01.52	5.1 ± 1.6	77.3 ± 1.5	M7	..
86	19 13 01.14	10 01 59.73	−0.9 ± 2.0	49.9 ± 0.3	M1	M7
87	19 14 14.14	10 28 02.55	4.6 ± 1.0	55.8 ± 0.6	M2.5	..
88	19 14 32.39	9 16 59.91	9.7 ± 2.6	45.1 ± 0.7	K5.5	M7
89	19 16 21.04	9 39 04.38	2.9 ± 1.0	48.4 ± 0.7	M0.5	M7
90	19 18 56.86	14 11 08.14	−1.0 ± 1.3	46.2 ± 0.3	M0	M7
91	19 21 44.57	13 37 22.45	4.6 ± 2.5	51.7 ± 0.4	M1.5	..
92	19 29 11.66	17 46 03.89	1.6 ± 2.2	44.3 ± 0.3	K5.5	M7
93	19 32 03.81	18 01 43.38	2.0 ± 2.2	50.5 ± 0.6	M1	..
94	19 41 53.19	22 41 36.64	8.4 ± 5.8	48.2 ± 1.1	M0.5	M7

Notes: (a)= Star #66 (2MASS J18442616-0335276) corresponds to the photometric candidate RSG A3 in Alicante 7 (Table 4 in Negueruela et al. 2011).